

Structure, Thermodynamics, and Solubility in Tetromino Fluids

Brian C. Barnes, Daniel W. Siderius, and Lev D. Gelb*

Department of Chemistry and Center for Materials Innovation, Washington University in St. Louis, St. Louis, Missouri 63130

Received January 16, 2009. Revised Manuscript Received March 4, 2009

To better understand the self-assembly of small molecules and nanoparticles adsorbed at interfaces, we have performed extensive Monte Carlo simulations of a simple lattice model based on the seven hard “tetrominoes”, connected shapes that occupy four lattice sites. The equations of state of the pure fluids and all of the binary mixtures are determined over a wide range of density, and a large selection of multicomponent mixtures are also studied at selected conditions. Calculations are performed in the grand canonical ensemble and are analogous to real systems in which molecules or nanoparticles reversibly adsorb to a surface or interface from a bulk reservoir. The model studied is athermal; objects in these simulations avoid overlap but otherwise do not interact. As a result, all of the behavior observed is entropically driven. The one-component fluids all exhibit marked self-ordering tendencies at higher densities, with quite complex structures formed in some cases. Significant clustering of objects with the same rotational state (orientation) is also observed in some of the pure fluids. In all of the binary mixtures, the two species are fully miscible at large scales, but exhibit strong species-specific clustering (segregation) at small scales. This behavior persists in multicomponent mixtures; even in seven-component mixtures of all the shapes there is significant association between objects of the same shape. To better understand these phenomena, we calculate the second virial coefficients of the tetrominoes and related quantities, extract thermodynamic volume of mixing data from the simulations of binary mixtures, and determine Henry’s law solubilities for each shape in a variety of solvents. The overall picture obtained is one in which complementarity of both the shapes of individual objects and the characteristic structures of different fluids are important in determining the overall behavior of a fluid of a given composition, with sometimes counterintuitive results. Finally, we note that no sharp phase transitions are observed but that this appears to be due to the small size of the objects considered. It is likely that complex phase behavior may be found in systems of larger polyominoes.

1. Introduction

The reversible self-assembly of objects of controlled size and shape is of great interest for the construction of nanoscale devices and nanostructured materials without laborious manipulation of individual particles. Self-assembly-based methods have been proposed, and in many cases demonstrated, for applications in areas from data storage¹ to medicine² to energy generation.³ Self-assembly occurs both at the molecular scale, most famously in self-assembled monolayers,^{4,5} and in nanoparticulate systems, polymers, and combinations of the two.^{6,7} Apart from its potential applications, self-assembly is also fascinating in its own right, with complex structures formed through an interplay of energetic and entropic forces. Studies of self-assembly relate naturally to work on the appearance and stabilization of structure in other systems, ranging from ordered crystals through partially ordered liquid crystals to disordered liquids.

Much insight into the structure and behavior of self-assembled systems, liquid crystals, and normal liquids has come from theoretical and simulation studies of idealized models. The simplest models are “hard”, or “athermal”, in that particles do not interact except to completely avoid overlap, behaving like

idealized billiard balls. In such systems the behavior is entropically controlled: the structure adopted by a system of rigid hard objects is that which maximizes the total entropy, a sum of translational and rotational contributions. Fluids of rigid hard objects studied to date have included disks,⁸ spheres,^{9,10} confined spheres,¹¹ hard dumbbells in two¹² and three¹³ dimensions, squares,¹⁴ rectangles,^{15–18} pentagons,¹⁹ rods, spherocylinders, and ellipsoids,^{20–22} cubes,²³ and others.

Lattice models, in which objects are positioned only at discrete sites, are appealing because of their simplicity, analytical tractability, and low computational cost. Hard sphere lattice systems have been studied with both analytical and numerical methods for

- (8) Metropolis, N.; Rosenbluth, A. W.; Rosenbluth, M. N.; Teller, A. H.; Teller, E. *J. Chem. Phys.* **1953**, *21*, 1087–1092.
- (9) Alder, B. J.; Wainwright, T. E. *J. Chem. Phys.* **1957**, *27*, 1208–1209.
- (10) Alder, B. J. *J. Chem. Phys.* **1964**, *40*, 2724–2730.
- (11) Siderius, D. W.; Corti, D. S. *Phys. Rev. E* **2007**, *75*, 011108.
- (12) Wojciechowski, K. W.; Frenkel, D.; Brańka, A. C. *Phys. Rev. Lett.* **1991**, *66*, 3168–3171.
- (13) Allen, M. P.; Imbierski, A. A. *Mol. Phys.* **1987**, *60*, 453–473.
- (14) Wojciechowski, K. W.; Frenkel, D. *Comput. Methods Sci. Technol.* **2004**, *10*, 235–255.
- (15) Porto, M.; Roman, H. E. *Phys. Rev. E* **2000**, *62*, 100–102.
- (16) Donev, A.; Burton, J.; Stillinger, F. H.; Torquato, S. *Phys. Rev. B* **2006**, *73*, 054109(11).
- (17) de las Heras, D.; Martínez-Ratón, Y.; Velasco, E. *Phys. Rev. E* **2007**, *76*, 031704.
- (18) Triplett, D. A.; Fichthorn, K. A. *Phys. Rev. E* **2008**, *77*, 011707(10).
- (19) Schilling, T.; Pronk, S.; Mulder, B.; Frenkel, D. *Phys. Rev. E* **2005**, *71*, 036138.
- (20) DeMiguel, E.; Rull, L. F.; Chalam, M. K.; Gubbins, K. E. *Mol. Phys.* **1991**, *74*, 405–424.
- (21) Bolhuis, P.; Frenkel, D. *J. Chem. Phys.* **1997**, *106*, 666–687.
- (22) McGrother, S. C.; Williamson, D. C.; Jackson, G. *J. Chem. Phys.* **1996**, *104*, 6755–6771.
- (23) Dijkstra, M.; Frenkel, D.; Hansen, J.-P. *J. Chem. Phys.* **1994**, *101*, 3179–3189.

*Corresponding author.

- (1) Bandić, Z. Z.; Litvinov, D.; Rooks, M. *MRS Bull.* **2008**, *33*, 831–837.
- (2) Gu, F.; Zhang, L.; Teply, B. A.; Mann, N.; Wang, A.; Radovic-Moreno, A. F.; Langer, R.; Farokhzad, O. C. *Proc. Natl. Acad. Sci. U.S.A.* **2008**, *105*, 2586–2591.
- (3) Schmidt-Mende, L.; Fechtenköter, A.; Müllen, K.; Moens, E.; Friend, R. H.; MacKenzie, J. D. *Science* **2001**, *293*, 1119–1122.
- (4) Ulman, A. *Chem. Rev.* **1996**, *96*, 1533–1554.
- (5) Love, J. C.; Estroff, L. A.; Kriebel, J. K.; Nuzzo, R. G.; Whitesides, G. M. *Chem. Rev.* **2005**, *105*, 1103–1170.
- (6) Glotzer, S. C.; Horsch, M. A.; Iacovella, C. R.; Zhang, Z. L.; Chan, E. R.; Zhang, X. *Curr. Opin. Colloid Int. Sci.* **2005**, *10*, 287–295.
- (7) Glotzer, S. C.; Solomon, M. J. *Nat. Mat.* **2007**, *6*, 557–562.

more than 40 years.^{24,25} Hard hexagons on a lattice were solved analytically by Baxter.²⁶ Freed and co-workers have studied the behavior of a variety of lattice objects, with and without energetic interactions, in the context of their “Lattice Cluster Theory”.^{27–29} Panagiotopoulos et al. have obtained the phase behavior of a variety of on-lattice shapes in three dimensions, both with nearest-neighbor attractive interactions and in the athermal limit. First-order crystallization transitions were recovered for on-lattice spheres and capped cylinders, while other rigid hard objects were found to display continuous order–disorder transitions.³⁰

Dill et al. have used both analytical methods³¹ and simulation³² to study solvation in fluids of hard lattice objects. Exact expressions for the partition functions of very small numbers of objects in a bounded domain were obtained using recursive methods. From these were obtained the equations of state (density vs chemical potential) of objects of several shapes, which were then analyzed in terms of Flory–Huggins theory and virial-like expansions.³¹ In the subsequent study,³² attractive interactions were added to the model and large-scale Monte Carlo simulations in the canonical ensemble used to extract relationships between the chemical potential of the fluid and its contact free energy per unit area, the latter being unambiguously definable in a lattice model. Analysis of fluid structure or the phase diagram of the model was not attempted.

Connected shapes on a two-dimensional lattice, as simulated above, are referred to in the mathematical literature as “polyominoes” and have been of interest for a considerable time.³³ Shapes that occupy one square are monominoes, those which occupy two are dominoes, etc. The mathematics of polyominoes has focused on two questions, the first being enumeration of the possible polyominoes occupying a given number of squares, and the second being the number of ways of arranging polyominoes in a bounded region, generalizing the question originally proposed as the number of possible placements of dominoes on a chessboard, also known as the “dimer model”.^{34,35}

Here we study self-assembly, liquid structure, and solvation in the multicomponent “tetromino” fluid using Monte Carlo simulations. There are seven different tetrominoes, corresponding to the shapes from the well-known computer game Tetris.³⁶ Although some of the tetrominoes (and various other polyominoes) have been simulated in the studies mentioned above,^{31,32,15} no comprehensive survey of the statistical mechanics or self-assembly of these objects seems to have been made to date. We note that related models have also been used in studies of compaction in granular matter^{37,38} and that the problem of arranging “falling polyominoes”, familiar from the computer

- (24) Gaunt, D. S.; Fisher, M. E. *J. Chem. Phys.* **1965**, *43*, 2840–2863.
- (25) Panagiotopoulos, A. Z. *J. Chem. Phys.* **2005**, *123*, 104504.
- (26) Baxter, R. J. *Exactly Solved Models in Statistical Mechanics*; Academic Press: London, U.K., 1982.
- (27) Li, W.; Freed, K. F.; Nemirovsky, A. M. *J. Chem. Phys.* **1993**, *98*, 8469–8483.
- (28) Buta, D.; Freed, K. F. *J. Chem. Phys.* **2002**, *116*, 10959–1096.
- (29) Buta, D.; Freed, K. F. *J. Chem. Phys.* **2004**, *120*, 6288–6298.
- (30) Davis, J. R.; Piccarreta, M. V.; Rauch, R. B.; Vanderlick, T. K.; Panagiotopoulos, A. Z. *Ind. Eng. Chem. Res.* **2006**, *45*, 5421–5425.
- (31) Kruckowski, A. E.; Chan, H. S.; Dill, K. A. *J. Chem. Phys.* **1995**, *103*, 10675–10688.
- (32) Brem, R.; Chan, H. S.; Dill, K. A. *J. Phys. Chem. B* **2000**, *104*, 7471–7482.
- (33) Golomb, S. W. *Polyominoes*, 2nd ed.; Princeton University Press: Princeton, NJ, 1994.
- (34) Kasteleyn, P. W. *Physica* **1961**, *27*, 1209–1225.
- (35) Cohn, H.; Kenyon, R.; Propp, J. *J. Amer. Math. Soc.* **2001**, *15*, 297–346.
- (36) Pajitnov, A. *Tetris*, computer game, 1985 (trademarked by The Tetris Co., LLC).
- (37) Caglioti, E.; Loreto, V.; Herrmann, H. J.; Nicodemi, M. *Phys. Rev. Lett.* **1997**, *79*, 1575–1578.
- (38) Krishnamurthy, S.; Loreto, V.; Herrmann, H. J.; Manna, S. S.; Roux, S. *Phys. Rev. Lett.* **1999**, *83*, 304–307.

game, is of practical interest as it is related to algorithms for the optimal packing of crates in trucks.³⁹ Finally, Cicoira and Rosei have drawn an analogy between the arrangement of pieces in Tetris and the self-assembly of molecules on surfaces,⁴⁰ and a version of tetrominoes augmented with energetic interactions has been studied in the context of self-organization by Troisi et al.⁴¹

We performed simulations in the grand canonical ensemble, corresponding to an open system. Because the model is two-dimensional, this is similar in spirit to experimental work on adsorption⁴⁰ and self-assembled monolayers.^{4,5} In such studies a surface is placed in contact with a solution or gas, from which particles (the solute, in the former case, and molecules of the gas, in the latter) reversibly adsorb to the surface. The surface layer is therefore in mass equilibrium with a reservoir of additional material; the concentration of the solution (or pressure, in the case of a gas) determines the coverage or density at the surface. Adsorption of molecules on surfaces also offers interesting possibilities for introducing and controlling chirality not present in three-dimensional systems.^{42,43}

The details of the model and simulations are discussed in section 2, followed by discussion of the structure of pure fluids (section 3.1), binary mixtures (section 3.2), and multicomponent mixtures (section 3.3). The interactions between different shapes are analyzed in terms of virial coefficients in section 3.4, followed by further analysis of solubility thermodynamics in both pure and multicomponent fluids in section 3.5, and a general discussion of these findings in section 4.

2. Methodology

2.1. Model. The objects (“pieces”) simulated are the seven possible “tetrominoes”, orthogonally connected objects that occupy four lattice sites. These shapes and their common names are given in Figure 1. The pieces interact only through avoidance of overlap; there is no attractive potential. There are two enantiomeric pairs: the S and Z shapes and the J and L shapes. These shapes are not chiral in three dimensions, but restriction to two dimensions eliminates some symmetry operations such that they are no longer superimposable. This is the complete set of “one-sided” tetrominoes, as opposed to the complete set of five “free” tetrominoes, which would exclude one of the enantiomers from each pair.³³ One could also consider simulations of larger polyomino sets, such as the 18 one-sided pentominoes or 60 one-sided hexominoes.

Further specifications are required for purposes of statistical mechanics. Only distinguishable rotations will be considered as available “states” for each shape, by analogy with the symmetry of molecules. Therefore, a square (O) has one rotational state, the rod (I), S, and Z pieces two states, and the J, L, and T pieces four states. As shown in Figure 1, each shape is given an “anchor point”, which will be used in the Monte Carlo simulations to define rotation and piece-insertion moves.

2.2. Simulation Details. In the grand canonical ensemble, the number of pieces of a given shape is not fixed but is controlled by an applied chemical potential. Simulations may include any number or combination of the seven shapes. Typically, grand canonical simulations of an *N*-component system sample an ensemble at constant temperature, volume, and the *N* chemical potentials $\{\mu_i\}$ or, equivalently, β , *V*, and the $N \{\beta \mu_i\}$, with

- (39) Coffman, E. G., Jr.; Downey, P. J.; Winkler, P. *Acta Inf.* **2002**, *38*, 673–693.
- (40) Cicoira, F.; Rosei, F. *Surf. Sci.* **2006**, *600*, 1–5.
- (41) Troisi, A.; Wong, V.; Ratner, M. A. *Proc. Natl. Acad. Sci. U.S.A.* **2005**, *102*, 255–260.
- (42) Liu, N.; Haq, S.; Darling, G. R.; Raval, R. *Angew. Chem., Int. Ed.* **2007**, *46*, 7913–7916.
- (43) Mao, L.; Harris, H. H.; Stine, K. J. *J. Chem. Inf. Comput. Sci.* **2002**, *42*, 1179–1184.

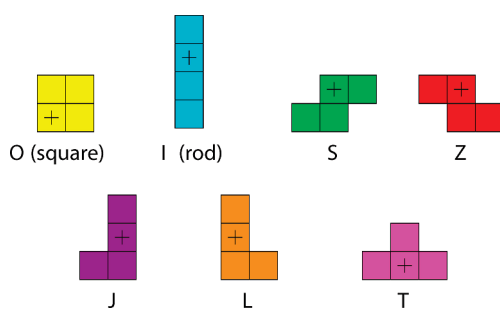


Figure 1. The seven one-sided tetrominoes, with corresponding names and symbols, and rotation centers/anchor points marked by “+” symbols. Orientations are labeled numerically, starting at 1. Squares have one orientation; rod, S, and Z shapes have two; J, L, and T shapes have four. The shapes shown are all in orientation 1; subsequent orientations correspond to 90° or 180° clockwise rotations around the marked points.

$\beta = 1/kT$. Because this is an athermal model, the temperature is an arbitrary parameter with no effect on the distribution of states, and so the thermodynamic variables are reduced to the volume and the $N\{\beta\mu_i\}$; we shall refer to these latter quantities as chemical potentials.

Our simulations include the following trial moves: insertions, deletions, translations, rotations, identity changes, and piece switches. With the exception of insertions, deletions, and identity changes, all of these are normal (that is, unbiased) Monte Carlo moves, such that the Boltzmann weight-based acceptance/rejection criteria are simply that moves which introduce an overlap are always rejected and moves which do not are always accepted. For insertion and deletion moves, we use a bias to improve sampling at high densities, similar to cavity bias insertion.⁴⁴ In this approach, a list of empty lattice sites is stored, and insertion attempts place a trial piece’s anchor point on one of those empty sites. The probability of accepting a piece insertion is then $\exp(\beta\mu_i) \times P_{\text{free}}/(N_i + 1)$, and the probability of accepting a deletion is $N_i/(\exp(\beta\mu_i) \times (P_{\text{free}} + 4))$, where N_i is the number of pieces of type i and P_{free} refers to the number of currently empty lattice points. This bias greatly increases efficiency at high densities by avoidance of trivially rejected insertion moves, while maintaining microscopic reversibility.

The other trial moves are straightforward. Translations consist of displacements of an entire piece by one lattice site, in one of the four Cartesian directions. Rotation moves consist of attempts to rotate a piece to a different distinguishable state, chosen randomly and uniformly from the other available states for the piece. Clearly, the location of the anchor point may affect the probability of a rotation attempt being accepted in dense configurations. The anchor points shown in Figure 1 were chosen near the center of each piece to provide more compact rotations that will likely result in fewer overlaps. Identity change moves attempt to both change the shape of a piece and its orientation. A piece of shape i is chosen at random and changed to a uniformly randomly selected different shape j and rotational state. Provided that no overlaps result, the move is accepted with probability $\exp(\beta\mu_j - \beta\mu_i) \times N_i/(N_j + 1)$. Note that the available shapes j are determined by those present in the simulation, that is, which have defined chemical potentials. “Piece switch” moves preserve both shape and rotational state. The locations of two pieces are switched, again using the anchor points to define the location of each piece. If there are no overlaps, the move is accepted.

In any multicomponent simulation, we attempt moves with relative frequencies of 3:3:9:2:2:1 (insertion:deletion:translation:rotation:identity change:piece switch). These weights were chosen as a compromise between efficiency at low and high densities. In simulations of one-component fluids, identity change and

piece switch moves were not used, and the relative frequencies of the remaining moves were unchanged. For simulations with at least one species at high chemical potential, insertion and deletion events tend to be infrequently accepted, and identity changes or piece switches become more important.

A simulation at a given state point consists of an equilibration phase followed by a data collection phase. For scans of many state points, the use of constant numbers of trial moves in the equilibration and data collection phases proved to be inefficient. We use automation and heuristics to determine when data collection can be begun at each state point and when sufficient statistical quality has been achieved such that a simulation can be terminated. All quantities to be evaluated, such as density and mole fraction, are tracked via the block-average method described by Flyvbjerg and Petersen.^{45,46} Each block contains 3000 samples, and each sample is separated by 1000 trial moves. The separation between samples was chosen to be on the order of the maximum number of pieces present in simulations at very high densities. The block length is chosen on the basis of preliminary runs and appears to provide reliable and uncorrelated block averages at all densities simulated. Data collection is not started until at least three blocks have been completed, and the density and other quantities have converged according to an exponential criterion, namely, $\ln(\rho_n/\rho_{n-1}) \leq 10^{-3}$, where ρ_n represents the average density of the system sampled during block n .

Simulation of an individual state point is terminated in one of two ways. Standard termination occurs when at least 500 million trial moves have been performed. Early termination occurs when the relative standard error of the density is below 0.001 (0.1%), the relative standard errors in the mole fractions of all components in a mixture are less than 0.2 (20%), and at least 10 blocks (30 million trial moves) of data collection have been completed. In practice, convergence of the density is the more stringent criterion. Under nearly all conditions mole fractions have converged to well within 0.01 (1%) by the time the density has converged; the only exceptions are in high-density mixtures where one component is of exceedingly low (< 0.01) mole fraction, for which quantity uncertainties of up to 0.15 (15%) are seen.

In our computer implementation the occupancies of all lattice sites are stored in a 512 byte integer vector, and bitwise operations are used to detect overlaps when trial moves are evaluated. This approach provides for very high efficiency and low memory footprint. On a modern processor (Intel Q9400, at 2.66 GHz), our code performs 2.36 million Monte Carlo trials per second (estimate obtained by averaging over simulations at low, medium, and high densities) and requires an average of 28 s to complete a simulation at a single state point. It is thus possible to survey large portions of the multicomponent phase space in reasonable time.

We have simulated systems ranging from pure species to seven-component mixtures. All single-component fluids were simulated over at least the chemical potential range -4.0 to $+8.0$ in increments of 0.2, for 61 total values per fluid. All 21 two-component (binary) mixtures were also simulated, with the chemical potential of each component scanned over the same range for a total of 3721 state points per two-component mixture. Mirror symmetry of enantiomers was not used to reduce the number of simulations required, partly for convenience and partly to illustrate the quality of the data obtained. All possible ternary (three-), quaternary (four-), quinary (five-), senary (six-), and septenary (seven-component) mixtures were simulated, but only along the phase space “diagonals” where all species have equal chemical potentials, $\beta\mu_i = \beta\mu_j = \beta\mu_k = \dots$, again scanned from -4.0 to $+8.0$. There are 35 each of ternary and quaternary mixtures, 21 each of binary and quinary mixtures, 7 senary mixtures, and a single septenary mixture.

(45) Flyvbjerg, H.; Petersen, H. G. *J. Chem. Phys.* **1989**, *91*, 461–466.

(46) Mignani, S.; Rosa, R. *Technometrics* **2001**, *43*, 347–355.

Simulations were performed on a 64×64 square lattice, under toroidal boundary conditions. A maximum of 1024 pieces can be present in a simulation cell of this size. To be confident this lattice was large enough that finite size effects were not significant, lattice sizes of 8×8 , 16×16 , 32×32 , and 48×48 were also tested. Properties such as the density and mole fractions were well-converged at the 64×64 lattice limit.

3. Results

3.1. Single-Component (Pure) Fluids. The packing fraction as a function of chemical potential, $\eta(\beta\mu)$, for all seven single-component fluids is given in Figure 2a, and the pressure plotted as a function of packing fraction, $\beta p(\eta)$, is given in Figure 2b; calculation of the pressure is described in the Appendix. The packing fraction is the fraction of lattice sites covered; each shape occupies four lattice sites, so the actual density (pieces per unit area) is one-fourth of this quantity. These data may be considered analogous to isotherms of $\rho(\mu)$ or $p(\rho)$ in a real system. The first form of the equation of state corresponds to the “raw” results of simulations in the grand ensemble, while the second corresponds to the way data are usually presented in studies using isothermal–isobaric and canonical ensemble simulations.¹² Again, simulations are performed from $\beta\mu = -4.0$ to $\beta\mu = 8.0$, corresponding to η ranging from below 0.10 to nearly 1.0 (complete filling). The isotherms for all shapes collapse onto a single curve at low chemical potentials. This is as expected; these are essentially gaseous systems with repulsive interactions and identical particle sizes and so should have very similar (although nonideal) gas-like behavior at low densities. This point will be revisited in section 3.4. At higher chemical potentials, the differences between the shapes become more apparent. At all chemical potentials squares (O shapes) exhibit higher density (or packing fraction) than all other shapes. Rods (I shapes) are the second densest and have density similar to that of the remaining shapes until $\beta\mu \approx -1.0$, after which they exhibit $\eta(\beta\mu)$ behavior rather more like that of the squares. The curves for S and Z shapes are identical because they are enantiomers, as are the curves for the J and L shapes. At the same chemical potential, S and Z fluids are slightly denser than J and L fluids, and the fluid of T shapes is the least dense at every chemical potential. In all cases, packing fractions smoothly approach the complete-filling limit at high chemical potential. The critical packing fraction for randomly placed small rectangles on a lattice is near 0.67,¹⁵ suggesting that these fluids must exhibit significant structure to achieve high densities. We have also obtained the isothermal compressibilities of all the pure fluids, which are entirely smooth and do not exhibit any significant features over this range of chemical potentials.

The smoothness of the density plots belies significant complexity in the structure of the fluids. Snapshots taken from simulations of the pure fluids are shown in Figures 3 and 4. In each case three snapshots are given, at chemical potentials corresponding to low, medium, and high densities. In the fluid of squares, there is little structure apparent in the snapshot at low density, other than that which might be expected from the non-overlap condition. In the medium-density snapshot, at a packing fraction of approximately 0.8, significant short-ranged structure is visible, with the pieces arranged in small, well-aligned groups. These tend to be three to six squares across at this density. The appearance and growth of these groups seems to correspond to the feature in the $\beta p(\eta)$ curves where the squares “break off” from the rods (Figure 2b). In the high-density snapshot, near 95% coverage, the squares form larger domains, some of which extend over the entire length of the

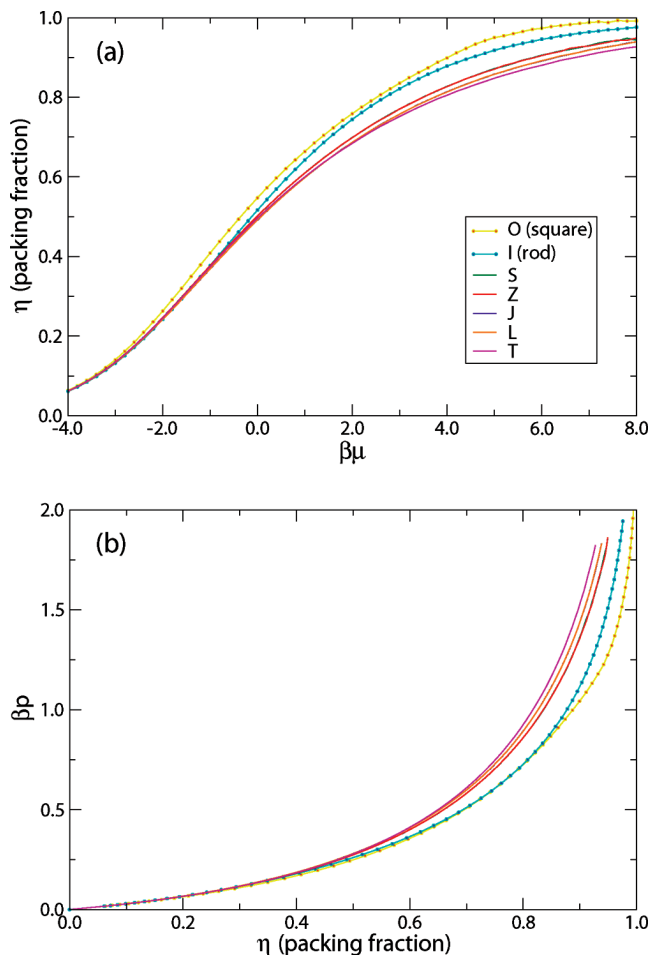


Figure 2. (a) Packing fraction η versus chemical potential $\beta\mu$ for one-component fluids. (b) Pressure βp versus packing fraction for one-component fluids. The color scheme in these plots is the same as for the shapes themselves (Figure 1).

simulation cell. We note that these structures break up and reform during the simulation. At these high densities a sort of one-dimensional ordering is observed in which the great majority of the pieces in the system are anchored on a lattice site with (in this case) an even-numbered y -coordinate; in the snapshot shown, only a few odd-anchored pieces are visible in the lower left. This behavior occurs because alignment in one direction increases translational mobility in the other, providing an overall entropic stabilization. As the packing fraction increases from 95% through 99.5%, this behavior becomes more prevalent and pronounced. While this is suggestive of the appearance of a true crystal phase, high-resolution scans in the chemical potential range of 4.0–6.0 do not show any signature of an abrupt transition and there is the likelihood that these structures are artificially stabilized by the periodic boundary conditions used. Similar “columnar” behavior has previously been observed in constant-pressure simulations of off-lattice hard squares. These also do not exhibit a true crystallization transition, and the columnar behavior is thought to be due to the influence of the periodic boundary conditions.¹⁴

The structure of the fluid of rods (I shapes) is rather different. In the snapshots shown in Figure 3, rods of vertical orientation are shown in a lighter color than rods of horizontal orientation, to highlight the orientational structuring present in this fluid. Even at low density, significant orientational correlation is present in the rod fluid, with neighboring rods tending to orient

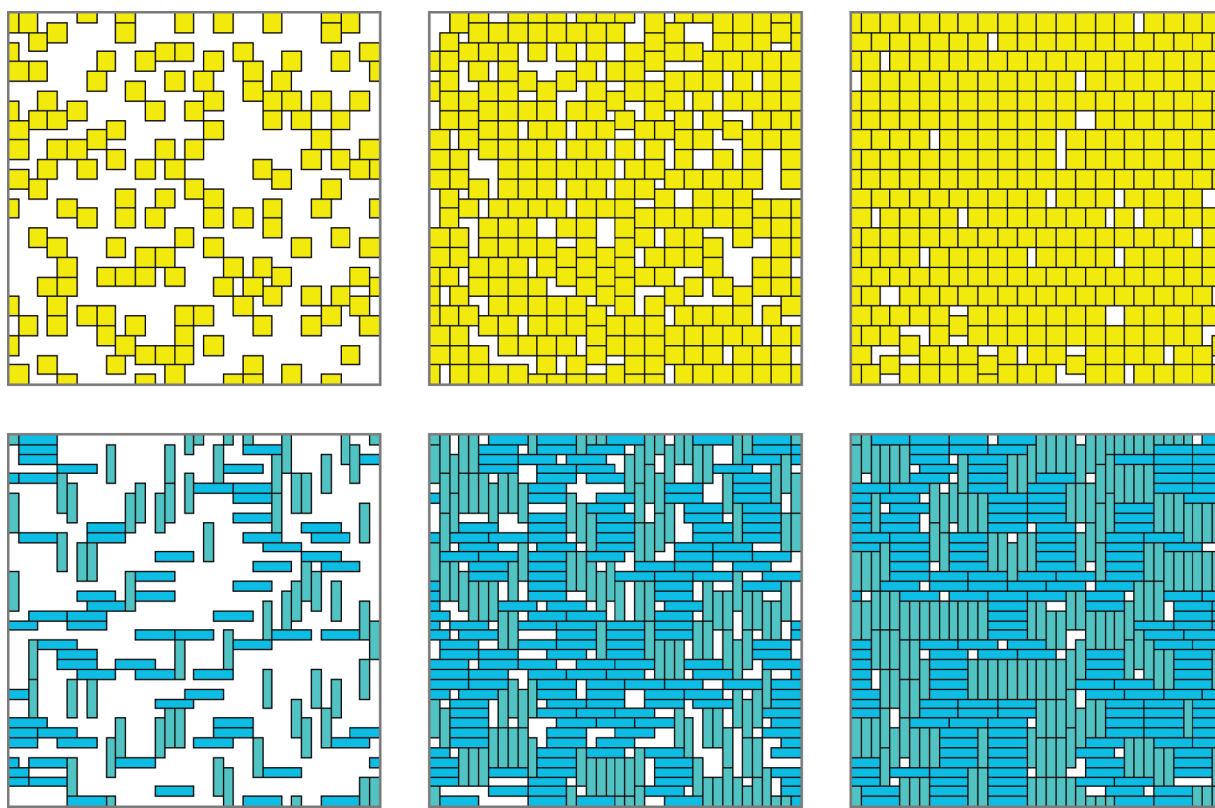


Figure 3. Configurations of pure fluids of squares and rods, at low (-1.0), medium ($+3.0$), and high ($+7.0$) chemical potentials. These are 38×38 sections cut from 64×64 simulation cells; as a result, pieces may extend over the boundary of the section shown. For the rods, which have two possible orientations, each orientation is shown in a slightly different color.

parallel to each other. This behavior suggests a possible transition to a nematic phase at higher densities, but in fact this does not occur. As the density increases, the local orientational correlation becomes stronger, but through a clustering mechanism that destroys any long-range correlation. In particular, at the middle density one observes clusters of approximately four parallel rods which are then oriented more-or-less randomly to each other. This behavior is similar to the “tetric” ordering observed in both off-lattice simulations of hard rectangles¹⁶ and in experimental work on a quasi-two-dimensional system of a monolayer of disk-shaped colloidal particles standing on edge.⁴⁷ However, particles in these systems can take any orientation, whereas the on-lattice nature of our simulations allows for only two orientations of the rod clusters (reinforcing tetric-like behavior), so the comparison is not wholly appropriate. At high density the clusters tend to grow somewhat larger, and a sort of layering is observed as they pack against like-oriented clusters. The apparent lack of an isotropic-to-nematic transition in this system is consistent with previous work. Ghosh and Dhar found that for packing fractions up to 0.85, only rods of length 7 or greater display an orienting transition on the square lattice;⁴⁸ we have performed additional calculations on rods of length 6 up to packing fractions of 0.99, and also found no transition.

A related kind of ordering is observed in the fluids of S and Z shapes, of which the S fluid is shown in Figure 4. Again, even at low densities, there is clearly short-range orientational order visible in the fluid, with pieces preferring to align parallel with each other. At the medium density, two kinds of local structure

are observed. In the first, and most common, neighboring pieces are offset in the diagonal ($\pm 1, \pm 1$) directions, which gives a “herringbone”-like structure. In the second, pieces are offset in the Cartesian directions ($0, \pm 1$) or ($\pm 1, 0$), depending on whether they are in the vertical or horizontal orientations, respectively. Interestingly, at higher densities, the Cartesian offset structure is largely suppressed in favor of the herringbone structure. As in the case of the rods, large domains of uniform alignment and greater positional regularity appear at high densities, but no sharp transition to a crystalline phase (ordered or not) is observed in the chemical potential range studied, and these domains remain much smaller than the system size.

The remaining shapes, the enantiomers J and L and the T shape, also display interesting orientational and positional ordering but of qualitatively different types, as shown in Figure 4. These shapes all have four distinguishable orientations, and unlike rod, S, and Z shapes, preferentially associate with pieces of orientation different from their own. We first consider the L fluid. At low density, L pieces are frequently found in a “stacked” configuration, with neighbors of the same orientation displaced by a single diagonal step on the lattice, much as in the S and Z fluids. However, at higher densities, L pieces begin to orient antiparallel with each other to form compact 2×4 site objects, which themselves pack efficiently along the Cartesian directions, much as in the fluids of squares and rods. The T fluid is also quite complex. At low densities, T shapes tend to be rotated 90° or 180° from their nearest neighbors. At higher densities, a prevalent packing motif appears to be a stack of several like-oriented pieces offset by the lattice vectors (0,2) or (2,0), with other pieces “fit” into the structure thus created in a less-regular way. Recall that the T fluid is the least dense of all the single-component fluids at a

(47) Zhao, K.; Harrison, C.; Huse, D.; Russel, W. B.; Chaikin, P. M. *Phys. Rev. E* **2007**, *76*, 040401R.

(48) Ghosh, A.; Dhar, D. *Eur. Phys. Lett.* **2007**, *78*, 20003.

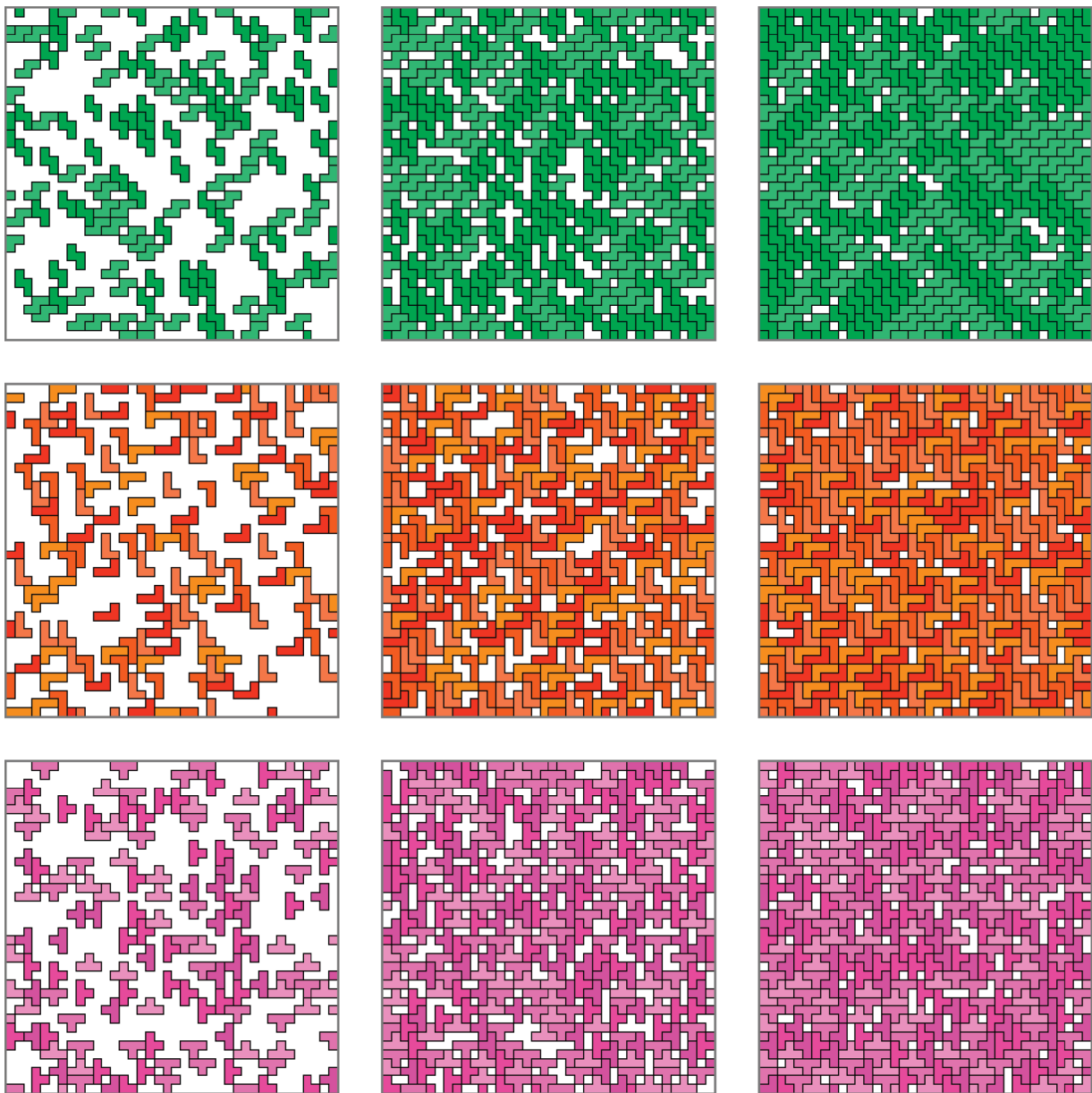


Figure 4. Configurations of pure fluids at low (-1.0), medium ($+3.0$), and high ($+7.0$) chemical potentials, for each of the S, L, and T shapes. These are 38×38 sections cut from 64×64 simulation cells; as a result, pieces may extend over the boundary of the section shown. As in Figure 3, each orientation is shown in a slightly different color.

given chemical potential. This appears to be because the T shapes are the most compact of the pieces with four orientations. Void spaces in the T fluid allow for much more orientational freedom than in, say, the L fluid, and the associated entropy drives the T fluid toward lower density.

3.2. Two-Component Systems. We have also scanned the phase space of all 21 binary mixtures, simulating a total of 78141 state points. In all cases, the two shapes were fully miscible over the chemical potential range simulated, but substantial nonideality was frequently observed, which we attribute to complex microscale fluid structure. Due to the large number of binary mixtures, only a selection of these systems will be discussed.

We first consider the two-dimensional equation of state $\eta(\beta\mu_i, \beta\mu_j)$, analogous to the isotherms of Figure 2 for one-component mixtures. Two of these are shown in Figure 5, as contour plots. In these plots, the lowest density is found in the lower left corner, at low chemical potential of both species, and the

highest density is found in the upper right corner, at high chemical potentials of both species. For species with similar properties, the plot should be approximately symmetric across the phase space diagonal $\beta\mu_i = \beta\mu_j$. In the square/rod mixture, substantial deviations from ideality are clearly evident. For example, the contour beginning at $\beta\mu_O = +6.5$ and $\beta\mu_I = -4.0$ gradually moves to higher $\beta\mu_O$ as $\beta\mu_I$ is increased. Equivalently, increasing $\beta\mu_O$ at constant $\beta\mu_I$ decreases the total system density. This is due to the rods disrupting the structure of the pure square fluid and corresponds to a positive volume of mixing (technically, area of mixing, because the system is two-dimensional). Of course, at sufficiently high $\beta\mu_I$ the total density must increase; this occurs here for $\beta\mu_I > 4.0$. A similar effect might be expected on the other side of the plot, where squares are introduced into a dense fluid of rods, but following the contour beginning near $\beta\mu_I = 6.0$ we see a much weaker effect. The difference between the effect of rods on the structure of the fluid of squares and the effect of squares on the structure of the fluid of rods can be seen in representative

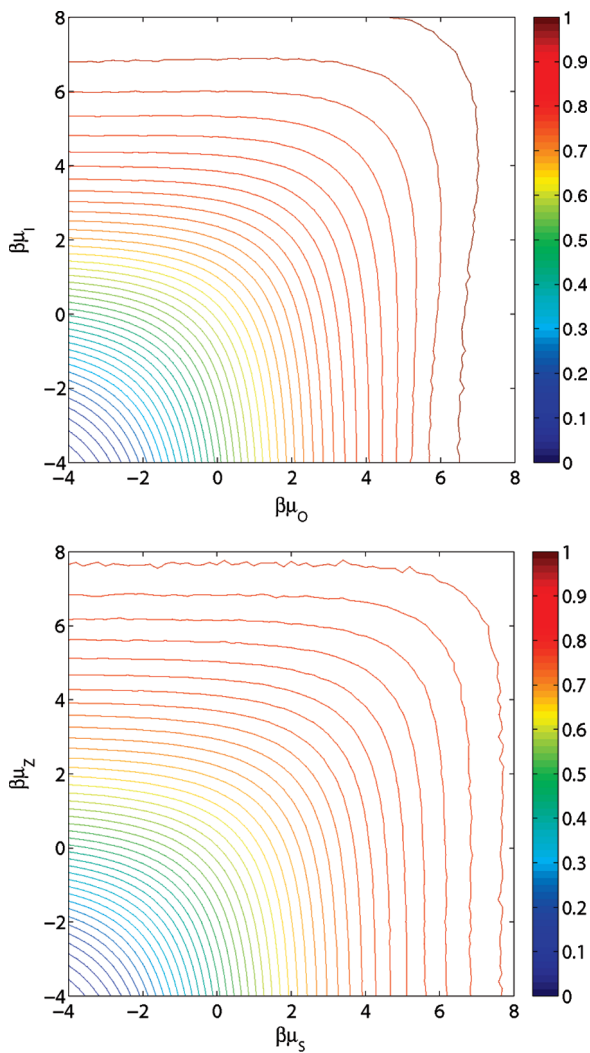


Figure 5. Contour plots of packing fraction versus chemical potentials for (top) mixtures of squares and rods and (bottom) mixtures of S and Z shapes.

snapshots, shown in Figure 6. In the former case, at high rod density and low square density, the squares seem to fit well into the rod fluid, the structure of which is generally similar to that seen in Figure 3. In the latter case, at low rod density and high square density, this is not the case. The rods, which span two or more rows of squares, induce alignment between the one-dimensional rows of squares described earlier. This reduces the entropy of the system and hence destabilizes it; the equilibrium density is thus lowered in compensation. Finally, the middle snapshot in Figure 3 is a mixture of squares and rods at the same chemical potentials (and nearly the same densities; the mole fraction of squares is 0.509 in the snapshot shown). Here the overall structure is dramatically perturbed, with both species still forming clusters, but of much smaller characteristic length scale.

The equation of state of the mixture of S and Z shapes (an enantiomeric pair), also shown in Figure 5, is necessarily symmetric about the $\beta\mu_S = \beta\mu_Z$ axis. The contours at high $\beta\mu_S$ and low $\beta\mu_Z$ are very nearly vertical, indicating that Z shapes are almost perfectly solvated by the S fluid; they simply replace S pieces and the density does not change. A configuration from a near-equimolar mixture of S and Z shapes is shown in Figure 7, in two different representations. As in the square/rod mixture, we see a dramatic tendency of the two species to segregate into “microclusters” (top image). This mixture displays

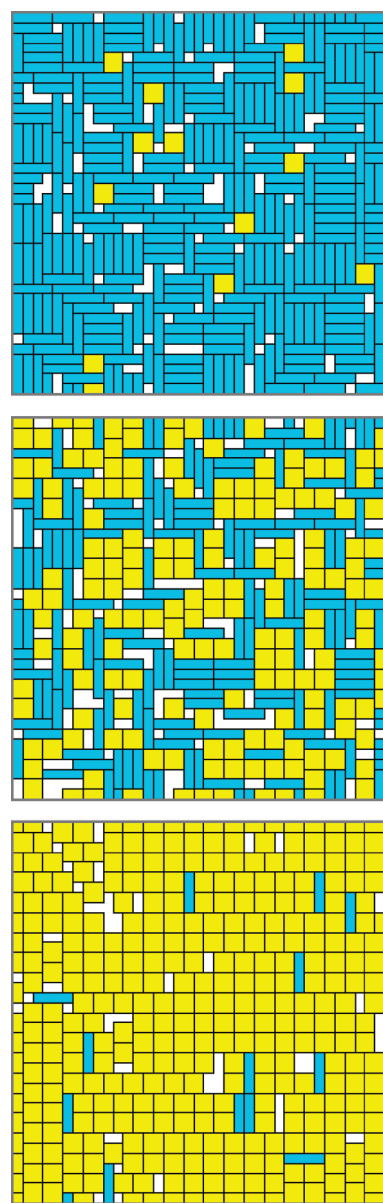


Figure 6. Snapshots taken from simulations of mixtures of squares and rods at (top) $\beta\mu_O = 0.0$ and $\beta\mu_L = 6.0$, (middle) $\beta\mu_O = \beta\mu_L = 4.0$, and (bottom) $\beta\mu_O = 6.0$ and $\beta\mu_L = 0.0$. These are 38×38 sections cut from 64×64 simulation cells; as a result, pieces may extend over the boundary of the section shown. Rods are all shown in the same color regardless of orientation.

herringbone-like structures as seen in the pure fluids, and the same sort of stacking motifs are also present. Interestingly, the bottom image in Figure 7 clearly indicates that the tendency of pieces of the same orientation to aggregate (as observed in Figure 4) is preserved in the mixture; individual S and Z pieces strongly prefer to associate with other pieces of both the same species and orientation. This behavior is further discussed in section 3.4.

Returning to the square/rod binary system, the structure of the fluid along the $\beta\mu_O = \beta\mu_L$ phase space diagonal (pictured in Figure 6) may be further analyzed in terms of average cluster size, shown in Figure 8. For these purposes we take two pieces of like species to belong to the same cluster if they touch along any face; pieces with only “corner contacts” are not considered to be part of the same cluster. We see in this figure that the average sizes of clusters of both shapes remain small even up to very high

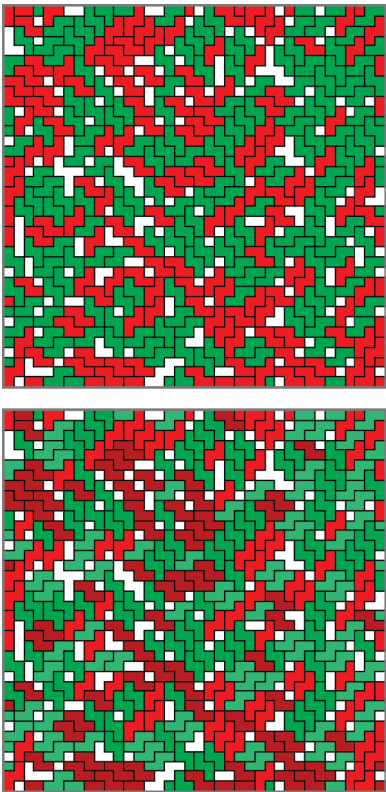


Figure 7. A single snapshot taken from a simulation of a mixture of S and Z shapes, at $\beta\mu_S = \beta\mu_Z = 4.0$, (top) without orientation-specific coloration and (bottom) with orientation-specific coloration.

densities, consistent with a picture of a globally well-mixed but locally clustered or phase-separated fluid. Interestingly, the rods form clusters that are over twice as large on average as those formed by squares. In the middle snapshot in Figure 6 we see, however, that the average size of the rod clusters is in fact misleading; the rods form a very large percolating cluster along with a number of very small isolated clusters. The clusters of squares, on the other hand, are distinct and well separated. The tendency of rod shapes to form large clusters was observed in all rod/shape binary pairs. However, a transferable hierarchy of cluster size is not otherwise present. For instance, while clusters of squares were largest in a square/S shape mixture, clusters of T shapes were largest in high-density square/T mixtures. However, in the S/T mixture, clusters of S shapes were consistently larger than clusters of T shapes.

To more deeply probe the nonideality of the binary mixtures, we have extracted the volume of mixing in each over the entire range of conditions simulated. These data, for selected binary systems, are shown in Figure 9. The conventional definition of the volume of mixing is

$$\Delta V_{\text{mix}}(\mathbf{N}, \beta p) = V(\mathbf{N}, \beta p) - \sum_i \hat{V}_i(\beta p) N_i \quad (1)$$

where \mathbf{N} is the vector quantity of N_i , the number of particles of each species, and $\hat{V}_i(\beta p)$ is the molar volume of pure species i at pressure βp . The data in Figure 9 are normalized by system volume and given as percentages, $(\Delta V_{\text{mix}}/V) \times 100\%$, plotted against pressure and mole fraction. The complete procedure for calculating the pressures and volumes of mixing is given in the Appendix. For an ideal solution, the volume of mixing is zero.

All of the binary systems in this model are nonideal, although to varying degree. The mixture of squares and rods is strongly

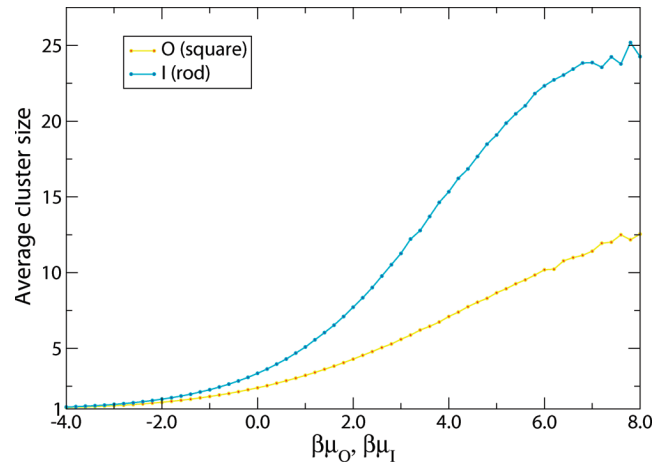


Figure 8. Average sizes of clusters of squares and rods in square/rod mixtures, along the $\beta\mu_O = \beta\mu_I$ phase space diagonal.

asymmetrical and peculiarly dependent on pressure, with a modest positive peak centered near $x_O = 0.7$ and $\beta p = 1.2$. This corresponds to the substantial deviation from ideality already seen in Figures 5 and 6, that introduction of rods into the square fluid at high density substantially perturbs the structure of that fluid, lowering the density (see Figure 5) until it is completely restructured near $x_O = 0.5$. At low pressure, however, the most positive volume of mixing occurs to the left of the $x_O = 0.5$ line, on the plateau located at $x_O = 0.4$ and $\beta p = 0.6$. The fluid density is much lower here, and this effect appears to be due to the presence of the squares interrupting the low-density orientational ordering behavior displayed in the pure rod fluid.

The square/S mixture is the most strongly nonideal of all the binary systems, with a dramatic peak in the volume of mixing observed at $x_O = 0.7$ and $\beta p = 1.2$. This peak is more than twice the height of that observed in the square/rod mixture. The reason for this is that the structures of the dense square fluid and the dense S fluid are fundamentally incompatible. The squares prefer to align along the Cartesian lattice directions with regular displacements of two lattice spacings, and clusters of squares have facets indexed along these lattice vectors. The S pieces prefer to align along the lattice diagonals, as discussed previously, and have facets indexed by the diagonal lattice vectors. It is impossible to create a fully rectilinear cluster of S shapes without vacancies. Therefore, one cannot pack clusters of squares and clusters of S shapes together without either introducing vacancies at the interface or perturbing the structure of the clusters. This leads to a very significant positive volume of mixing of these fluids. Again, this effect is asymmetric across the $x_O = 0.5$ line, with squares clearly more compatible with (less perturbing to) the structure of the S fluid than vice versa, much as in the square/rod mixture.

Rods and Z shapes display the second largest positive volume of mixing of the systems shown, although at somewhat lower pressures and near equimolarity. Rods are somewhat more compatible with the Z (or S) fluid than are squares, because rod clusters are better able to distort and accommodate the characteristic diagonal facets of clusters of Z shapes. Nonetheless, this disrupts the rods' tendency to form small clusters aligned in both directions. This incurs a free energy cost, which the system alleviates by increasing the total volume, corresponding to $\Delta V_{\text{mix}} > 0$.

Of the remaining binary systems shown, rods and T shapes are most strongly nonideal at pressures near 0.5, suggesting that the structures of these two fluids at even modest packing fractions (near 0.7) are particularly incompatible. At higher pressures, the

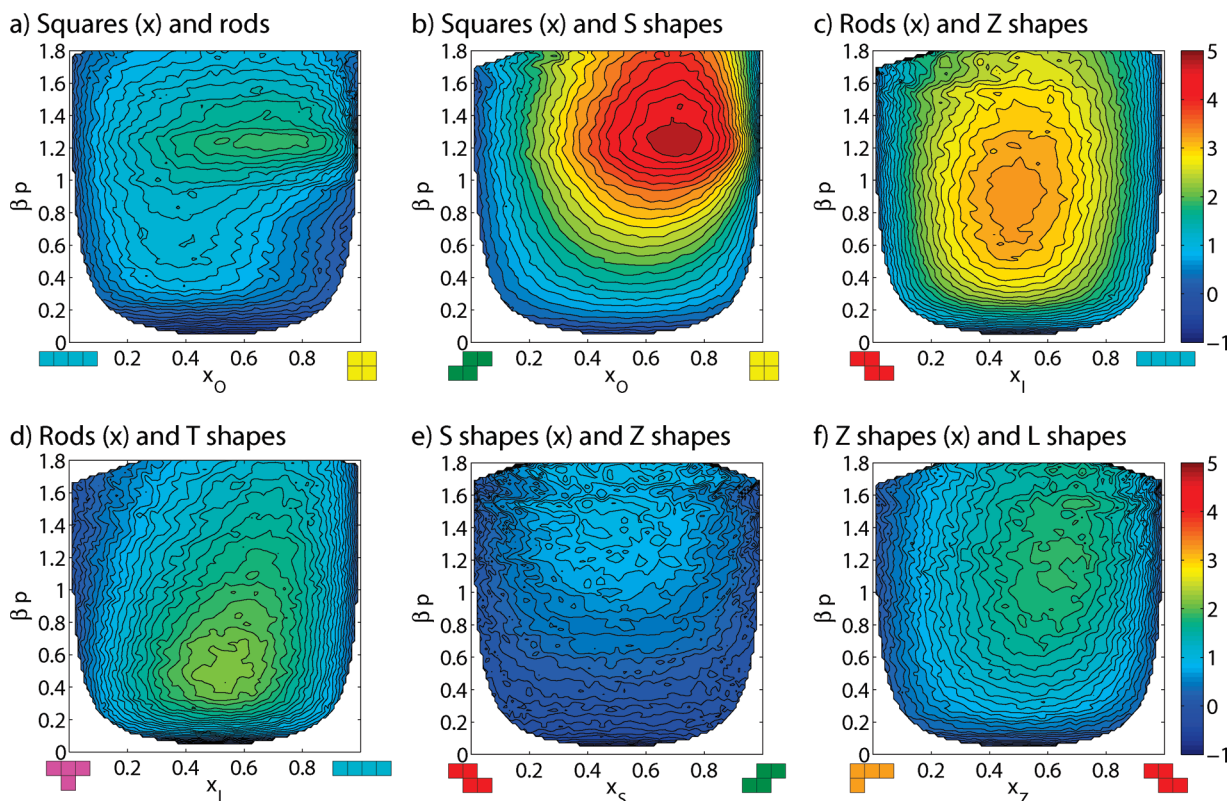


Figure 9. Contour plots of volume of mixing versus pressure βp and mole fraction x for various binary mixtures: (a) squares and rods, (b) squares and S shapes, (c) rods and Z shapes, (d) rods and T shapes, (e) S shapes and Z shapes, and (f) Z shapes and L shapes. In all cases the mole fraction shown is that of the first shape of the pair. All figures are plotted on the same vertical scale, in relative percentage units, $(\Delta V_{\text{mix}}/V) \times 100\%$.

peak in volume of mixing shifts to $x_1 > 0.5$, suggesting that T shapes are less soluble in the rod fluid than are rods in the T fluid. The mixture of Z and L shapes is closer to ideal than any of those discussed so far, with a broad but low peak shifted slightly to the Z-rich side of the diagram. Finally, the mixture of S and Z shapes, already considered in Figures 5 and 7, is of course symmetric about $x_S = 0.5$ and shows only very slightly positive volume of mixing at very high pressures, even while displaying significant microscopic segregation (Figure 7).

Mixtures containing rods exhibit ΔV_{mix} maxima at generally lower pressures than other mixtures. In Figure 9 this is particularly evident for the rod/T mixture and the rod/Z mixture, but it is also true for rods and squares and the rod/L mixture not shown. This is another consequence of the pronounced local ordering that occurs in the rod fluid at lower densities (Figure 3). Finally, we note that at very low pressures and/or at mole fractions very close to 1 or 0, many mixtures appear to display negative volumes of mixing. We are confident that this is a numerical artifact. Under these conditions the molar volume in one or both pure fluids becomes extremely large, and the correspondingly large statistical error in these quantities leads to large uncertainty in the (near-zero) volume of mixing. Note that it is possible for binary mixtures such as these to display a negative volume of mixing, however, as discussed below in section 3.4.

3.3. Many-Component Systems. We have simulated all multicomponent systems at many state points along the phase space diagonal and found that the tendency of shapes to self-associate persists even when many components are present. To illustrate this behavior, snapshots from simulations of selected three-, four-, five-, six-, and seven-component mixtures at high densities ($\beta\mu = 7.0$) are shown in Figure 10. In all cases, clusters of each species are readily apparent, which is true in every

multicomponent mixture that we have visualized. As in the binary mixtures, pieces are well-mixed at large length scales, and we have no evidence for any sort of first-order fluid–fluid transition in these systems. Furthermore, even when many different shapes are present, there is no tendency to form clusters or characteristic structures composed of more than one shape.

We have obtained the average sizes of the clusters of each shape in each of these simulations, shown in Table 1. As the number of components increases, the average size of clusters of a given species decreases. Most of this effect is simply due to dilution; the tendency to form clusters must be significantly reduced as the number of particles of a given shape decreases. For instance, in the S/Z/T ternary mixture, the average size of S (or Z) clusters at high pressure reaches as high as 3.364, while in the O/I/S/Z/J/L senary mixture, it is reduced to very nearly half that value, 1.628. There is nonetheless significant information contained in the cluster size data. In the two systems containing rods, the clusters of rods are substantially larger than those of other shapes. One might suspect that this is simply due to the ability of rods to make contacts at larger separation than other pieces. However, upon inspection of the snapshots in Figure 10, we see that rod clusters tend to be closely packed rather than extended, which suggests that in fact the rods aggregate more strongly than the other shapes. In the S/Z/J/T quaternary mixture, the S and Z cluster sizes differ by a statistically significant 0.036, whereas in the S/Z/T ternary mixture they are the same to within the uncertainty of the measurement. This is a result of the two enantiomers interacting differently with the (also chiral) J shape in the quaternary mixture. In the senary and septenary mixtures shown, both members of each chiral pair are present, and there is no enantiomeric resolution. Finally, in the two systems containing squares, squares form larger clusters

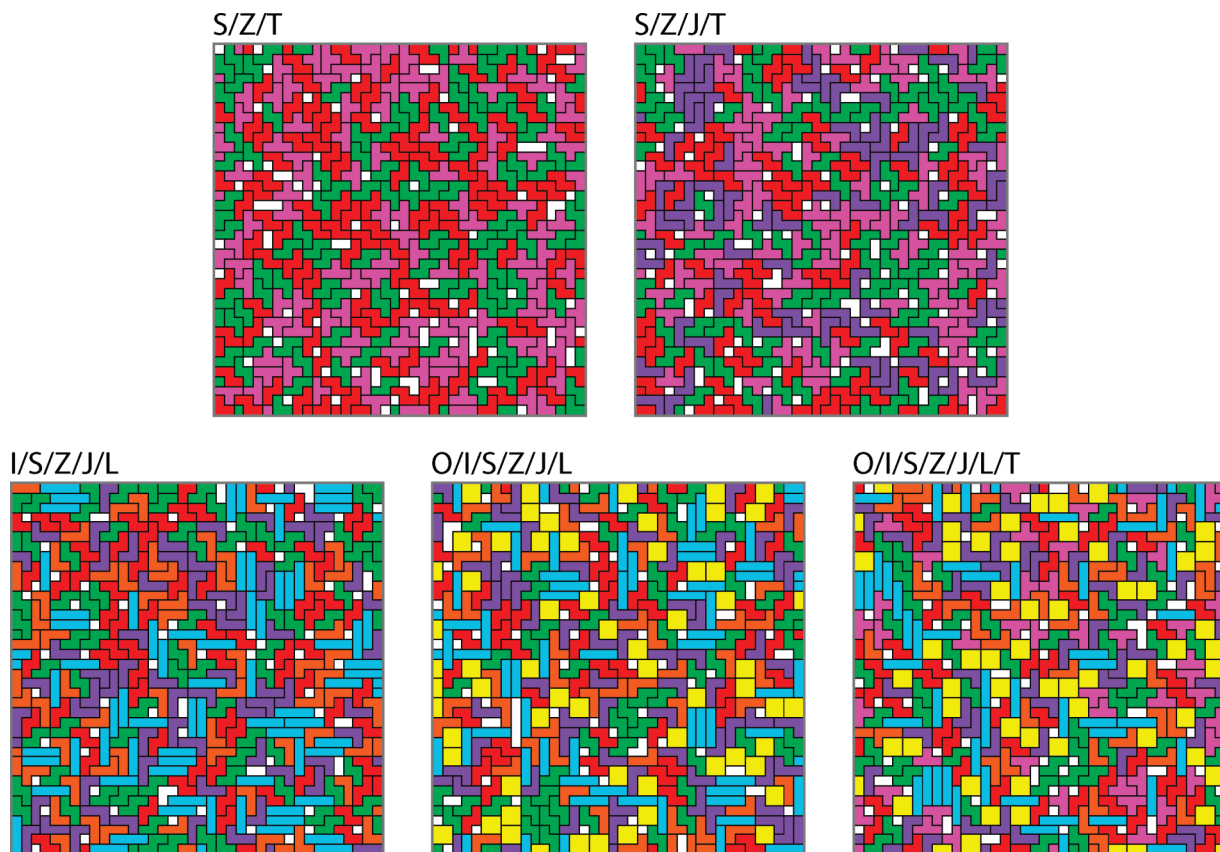


Figure 10. Representative snapshots of selected three-, four-, five-, six-, and seven-component mixtures, with all species at $\beta\mu = 7.0$. These are 38×38 sections cut from 64×64 simulation cells; as a result, pieces may extend over the boundary of the section shown. All pieces of a given shape are shown in the same color, regardless of orientation.

Table 1. Average Size of Clusters of Each Shape, from Simulations at $\beta\mu_i = 7.0$ for All i , for the Mixtures Shown in Figures 6 and 10^a

mixture	average size of clusters of						
	species O	species I	species S	species Z	species J	species L	species T
O/I	11.407	24.041					
S/Z/T			3.354	3.364			2.962
S/Z/J/T			2.284	2.248	2.415		2.181
I/S/Z/J/T		2.450	1.826	1.828	1.932	1.933	
O/I/S/Z/J/L	1.769	2.051	1.628	1.628	1.703	1.698	
O/I/S/Z/J/L/T	1.608	1.836	1.517	1.518	1.568	1.570	1.550

^aStatistical uncertainty in these data is ± 0.005 at 95% confidence.

than any other shape besides rods, despite the compactness of the squares reducing their ability to make contacts at large distance.

An approximate combinatorial argument can provide further insight regarding the mean cluster sizes. In the dense fluids shown in Figure 10, nearly all pieces have four, five, or six neighbors. We can make an approximate prediction of the average cluster size in a “well-mixed” equimolar fluid by using combinatorics to predict the probability that a randomly chosen particle will have a certain number of neighbors of the same shape as itself, and then using these values as estimates of the probability distribution of different cluster sizes. For an exactly equimolar seven-component mixture, assuming that each piece has six neighbors, the probability that a chosen piece has zero “like” neighbors is approximately 0.396, the probability of one “like” neighbor is also 0.396, and the probability of two “like” neighbors is 0.165. Assuming that this is also the distribution of clusters of one, two, and three pieces, respectively, we obtain an average cluster size of 1.50.

Table 2. Matrix of Second Virial Coefficients^a

B_{ij}	O	I	S	Z	J	L	T
O	4.50	5.00	5.00	5.00	5.00	5.00	5.00
I	5.00	5.75	5.75	5.75	5.75	5.75	5.75
S	5.00	5.75	5.25	5.25	5.50	5.50	5.25
Z	5.00	5.75	5.25	5.25	5.50	5.50	5.25
J	5.00	5.75	5.50	5.50	5.50	5.625	5.50
L	5.00	5.75	5.50	5.50	5.625	5.50	5.50
T	5.00	5.75	5.25	5.25	5.50	5.50	5.25

^aNote that these coefficients are exact.

If each piece has only five neighbors, then the average cluster size predicted in this way is 1.39; for pieces with four neighbors, 1.32. Such a simple argument will underpredict the average cluster size, but not by a large amount; a “well-mixed” fluid should therefore be expected to have average cluster sizes near 1.4. Significantly, in the simulated seven-component mixture, all shapes have average cluster sizes larger than this, with squares and rods in particular forming much larger clusters than would

Table 3. Matrix of Orientation-Specific Second Virial Coefficients^a

B_{ij}'	O1	I1	I2	S1	S2	Z1	Z2	J1	J2	J3	J4	L1	L2	L3	L4	T1	T2	T3	T4
O1	4.5	5.0	5.0	5.0	5.0	5.0	5.0	5.0	5.0	5.0	5.0	5.0	5.0	5.0	5.0	5.0	5.0	5.0	5.0
I1	5.0	3.5	8.0	6.5	5.0	6.5	5.0	5.0	6.5	5.0	6.5	5.0	6.5	5.0	6.5	6.5	5.0	6.5	5.0
I2	5.0	8.0	3.5	5.0	6.5	5.0	6.5	6.5	5.0	6.5	5.0	6.5	5.0	6.5	5.0	6.5	5.0	6.5	5.0
S1	5.0	6.5	5.0	4.5	6.0	5.5	5.0	5.5	5.5	5.5	5.5	6.0	5.0	6.0	5.0	5.0	5.5	5.0	5.5
S2	5.0	5.0	6.5	6.0	4.5	5.0	5.5	5.5	5.5	5.5	5.5	5.0	6.0	5.0	6.0	5.5	5.0	5.5	5.0
Z1	5.0	6.5	5.0	5.5	5.0	4.5	6.0	6.0	5.0	6.0	5.0	5.5	5.5	5.5	5.5	5.0	5.5	5.0	5.5
Z2	5.0	5.0	6.5	5.0	5.5	6.0	4.5	5.0	6.0	5.0	6.0	5.5	5.5	5.5	5.5	5.5	5.0	5.5	5.0
J1	5.0	5.0	6.5	5.5	5.5	6.0	5.0	5.5	6.0	4.5	6.0	5.5	5.5	5.5	6.0	6.0	5.0	5.5	5.5
J2	5.0	6.5	5.0	5.5	5.5	5.0	6.0	6.0	5.5	6.0	4.5	6.0	5.5	5.5	5.5	5.5	6.0	5.0	5.5
J3	5.0	5.0	6.5	5.5	5.5	6.0	5.0	4.5	6.0	5.5	6.0	5.5	6.0	5.5	5.5	5.5	5.5	6.0	5.0
J4	5.0	6.5	5.0	5.5	5.5	5.0	6.0	6.0	4.5	6.0	5.5	5.5	5.5	6.0	5.5	5.0	5.5	5.5	6.0
L1	5.0	5.0	6.5	6.0	5.0	5.5	5.5	5.5	6.0	5.5	5.5	5.5	6.0	4.5	6.0	6.0	5.5	5.5	5.0
L2	5.0	6.5	5.0	5.0	6.0	5.5	5.5	5.5	5.5	6.0	5.5	6.0	5.5	6.0	4.5	5.0	6.0	5.5	5.5
L3	5.0	5.0	6.5	6.0	5.0	5.5	5.5	5.5	5.5	5.5	6.0	4.5	6.0	5.5	6.0	5.5	5.0	6.0	5.5
L4	5.0	6.5	5.0	5.0	6.0	5.5	5.5	6.0	5.5	5.5	5.5	6.0	4.5	6.0	5.5	5.5	5.5	5.0	6.0
T1	5.0	5.0	6.5	5.0	5.5	5.0	5.5	6.0	5.5	5.5	5.5	6.0	5.0	5.5	5.5	5.5	4.5	5.5	5.5
T2	5.0	6.5	5.0	5.5	5.0	5.5	5.0	5.0	6.0	5.5	5.5	5.5	6.0	5.0	5.5	5.5	5.5	4.5	5.5
T3	5.0	5.0	6.5	5.0	5.5	5.0	5.5	5.5	5.0	6.0	5.5	5.5	6.0	5.0	4.5	5.5	5.5	5.5	5.5
T4	5.0	6.5	5.0	5.5	5.0	5.5	5.0	5.5	5.5	5.0	6.0	5.5	5.5	6.0	5.5	4.5	5.5	5.5	5.5

^aThe orientations of each piece are numbered according to the scheme described in Figure 1. These coefficients are exact.

be expected from random placement. In the seven-component mixture, then, all of these shapes prefer to self-associate.

3.4. Analysis of Virial Coefficients. To better understand the interactions between different shapes, we have calculated all of the second virial coefficients B_{ij} , as defined by the expansion of the pressure of a binary i,j mixture in powers of the densities of both species:

$$\beta p = \rho_i + \rho_j + B_{ii}\rho_i^2 + 2B_{ij}\rho_i\rho_j + B_{jj}\rho_j^2 + \dots \quad (2)$$

These are obtained from the lattice analogue of a cluster integral^{49,50}

$$B_{ij} = -\frac{1}{2} \sum_k f_{ij}(k) \quad (3)$$

where $f_{ij}(k) = 0$ if pieces of types i and j do not overlap if placed in a configuration indexed by k and $f_{ij}(k) = -1$ if they do overlap. In the summation, k runs over all possible configurations (that is, orientations and relative displacements) of two pieces. Because the number of such configurations is enumerable, this sum can be evaluated exactly; the resulting B_{ij} values are shown in Table 2. Likewise, an “orientation-specific virial coefficient” B_{ij}' is defined by taking the two pieces in specific orientations and only summing over relative displacements. These orientation-specific coefficients are shown in Table 3.

The B_{ij} are clearly measures of how “strongly” two pieces overlap. They are all necessarily positive and contribute to increasing the pressure of a fluid over its ideal value. Low values may be interpreted as indicating a more “favorable” interaction than high values, although of course there is no direct attraction between any of the shapes. In the B_{ij} matrix of Table 2, a variety of interesting features are seen. Consider first the diagonal values, corresponding to the second virial coefficients of the seven pure fluids. These are all of the same magnitude, because

the shapes all occupy the same number of sites and have similar lateral extent. Nonetheless, the variation is significant. The value for squares, $B_{OO} = 4.5$, is the lowest, while the value for rods, $B_{II} = 5.75$, is the highest. Of the remaining, the S, Z, and T values of 5.25 are slightly lower than the J and L values of 5.5. One would expect, on the basis of these data, that the squares would have the highest density at a given pressure, followed in turn by S, Z, and T, J and L, and finally the rods. While the squares do in fact have the highest density at a given pressure, this argument fails to predict the high density of the rods and does not distinguish between the S (or Z) and T shapes at all. Another feature of these data is that the B_{OX} all have the same value for $X \neq O$, which is due to the squares having higher symmetry than any other shape. Interestingly, all of the B_{IX} are the same for $X \neq I$ and $X \neq O$, and rods have the second highest symmetry.

Likewise, the B_{ij}' clearly do not tell the whole story in regard to the behavior of binary mixtures. For example, while the B_{IZ} value of 5.75 is certainly larger than $B_{ZZ} = 5.25$, it is the same as the coefficient for pure rods and does not seem to correlate with the significant positive volume of mixing seen in Figure 9. The coefficient for squares and S shapes, $B_{OS} = 5.0$, is smaller even than $B_{SS} = 5.25$, which does not correlate at all with the extremely large positive volume of mixing in this system. To better understand these effects we turn to the orientation-specific coefficients B_{ij}' in Table 3.

First, the two values for B_{II}' explain the discrepancy of the density of the rod fluid and the high value of B_{II} . Like-aligned rods have $B' = 3.5$, the lowest value on the table, while unlike-aligned rods have $B' = 8.0$, the highest. The average of these two gives the high $B_{II}' = 5.75$, but because there is significant orientational clustering in the rod fluid, the “effective” value should be much lower (closer to 3.5), accounting for the very high density of this fluid. For the pure S (and Z) fluids, we see that again the diagonal values of $B' = 4.5$ are lower than the off-diagonal values of $B' = 6.0$, in accord with the earlier observation that these pieces tend to form clusters with all pieces in the same orientation. In the pure J and L fluids, different behavior is observed. Of the four orientations, each prefers to associate with (that is, has the lowest B' value for) the 180° rotation of itself.

(49) Hill, T. L. *An Introduction to Statistical Thermodynamics*; Addison-Wesley: Reading, MA, 1960.

(50) Moghaddam, S.; Kim, Y. C.; Fisher, M. E. *J. Phys. Chem. B* **2005**, *109*, 6824–6837.

Table 4. Solubility ($1/\beta K_i$) of Each Shape in Various Solvents at $\beta p = 0.5^a$

solvent	η_s	solute species					
		O	I	S	Z	J	T
O	0.696		0.218	0.168	0.168	0.196	0.196
I	0.694	0.232		0.146	0.146	0.159	0.159
S	0.660	0.227	0.147		0.210	0.168	0.174
Z	0.660	0.226	0.146	0.210		0.174	0.168
J	0.653	0.267	0.185	0.185	0.191		0.178
L	0.653	0.267	0.185	0.191	0.184	0.178	
T	0.650	0.243	0.167	0.212	0.212	0.182	0.182
O/T	0.664		0.193	0.202	0.202	0.195	0.195
S/J	0.647	0.256	0.174		0.206		0.185
L/T	0.646	0.256	0.179	0.207	0.202	0.183	
senary	0.649–0.656	0.253	0.176	0.192	0.192	0.185	0.184
average		0.244	0.175	0.185	0.185	0.176	0.182

^a Values given are certain to within ± 0.002 . The first column contains the packing fraction of the solvent, η_s . The first seven rows of the table show the solubility of each shape in the pure fluids of each other shape. The diagonal values are missing because Henry's law does not apply to components of the solvent. The next three rows show the solubility of various shapes in each of three binary mixtures, with both mixture components at the same chemical potential. The row labeled "senary" shows the solubility of each shape in a six-component mixture composed of all the other shapes, again all at the same chemical potential and $\beta p = 0.5$; these solvents do not all have the same packing fraction, but they vary over only a small range, given in the η_s column. The final row gives the average of the solubility of each shape in the six other pure solvents; note that this quantity does not have a rigorous thermodynamic interpretation and is only given for the sake of comparison.

That is, J1 and J3 are a preferentially associating pair, with $B' = 4.5$, as are J2 and J4. This, again, is consistent with the behavior seen in the snapshots of Figure 4. The $Ji-Jj$ association, corresponding to the diagonal-offset "stacking" seen at low densities, has $B' = 5.5$, the second lowest value. The 90° associations (J1–J2, etc.) are the least favorable and are less common in the snapshots. Finally, somewhat similar behavior is observed in the pure T fluid, with a strong preference for the T1–T3 and T2–T4 associations, with $B' = 4.5$, over all others, with $B' = 5.5$.

Considering the B_{ij} and B_{ij}' values for $i \neq j$, we see that, whereas the B_{ij} values suggest possibly favorable associations between pieces of different shape, taking orientation into account shows a substantially different picture. The lowest B' for any binary mixture is 5.0, while for every pure species there is at least one value of 4.5 or below. This suggests that every shape packs better with its own kind than with any other, provided they are allowed to adopt favorable orientations.

Although the strongest associations are between pieces of the same shape (but not necessarily in the same orientation), in binary mixtures there are still preferred orientations for associations between pieces of different shape. For example, for neighboring S and Z pieces, the preferred orientations are between the pairs S0–Z1 and S1–Z0, that is, with one piece turned 90° to the other. In fact, looking at the snapshot in Figure 7 this motif is often, although not always, adopted at the interface between clusters of S shapes and clusters of Z shapes. We also see significant differences between interactions of enantiomers; the S–J coefficients (equal to those of the Z–L pair, of course) are substantially different from the S–L (Z–J) ones. The S–J coefficients are all the same, $B' = 5.5$, in fact, while in the S–L case there is orientational preference, with S1 pieces preferring association with L2 and L4 ($B' = 5.0$) over association with L1 and L3 ($B' = 6.0$). This reflects the enantiomeric resolution discussed earlier.

Finally, we note that it is possible in this system to obtain a negative volume of mixing at pressures sufficiently low that the virial equation of state truncated at second order is accurate. We have verified numerically that this occurs in the rod/square mixture. The requirement of accuracy at second order means that the effect is seen only at extremely low pressures and

densities and is therefore very small; nonetheless, it is curious to see a negative volume of mixing between two dilute gases with purely repulsive interactions.

3.5. Solubility and Solvation. To further probe the interaction between different shapes we turn to Henry's law coefficients, which measure the solubility of one species in a fluid composed of others. The Henry's law constant K_i for solute i in a given solvent is defined by $f_i^\infty(T,p,x_i) = x_i K_i(T,p)$, where x_i is the mole fraction of species i and f_i^∞ is the fugacity of species i at infinite dilution, which in a real liquid is similar to its partial pressure in the coexisting vapor. In our athermal model, this becomes $\beta f_i^\infty(\beta p, x_i) = x_i \beta K_i(\beta p)$. βK_i measures the ratio of fugacity to mole fraction for the solute at infinite dilution; when its value is very small, species i is very soluble, and when its value is large, species i is very insoluble. The inverse quantity $1/\beta K_i$, therefore, is a measure of solubility: it reports the mole fraction of solute that would be attained at unit solute fugacity (partial pressure) if the Henry's law region extended to such high mole fraction.⁵¹ In fact, simulations indicate that these systems display Henry's law behavior only for mole fractions significantly below $x = 0.001$, indicating strong nonideality. We have measured these constants for each shape dissolved in each pure fluid and in a number of multicomponent solvents, all at several pressures. The details of this calculation are given in the Appendix. A selection of these data at $\beta p = 0.5$ are shown in Table 4. This pressure corresponds to packing fractions near 0.65 for all of the solvents considered. We first consider the various shapes dissolved in pure fluids. Overall, squares are always the most soluble, and rods are usually the least soluble. There is significant variation from solvent to solvent, however. Squares are themselves most soluble in the J and L fluids and least soluble in the S and Z fluids. The latter is consistent with the large volume of mixing of squares and S shapes seen in Figure 9, which indicates poor compatibility between those two shapes. However, such behavior would not have been predicted from the virial coefficients; the cross-coefficients for squares and S, Z, J,

(51) A common, although less rigorous, formulation of Henry's law is written $c_i = k_H p_i$, reflecting its original discovery.⁵² Here, large values of the constant k_H indicate high molar concentration c_i at given partial pressure p_i ; k_H is thus analogous to our $1/\beta K_i$.

(52) Henry, W. *Philos. Trans. R. Soc. (London)* **1803**, 93, 29–43.

and L shapes are all the same. Rods, on the other hand, are most soluble in the fluid of squares, followed by the fluids of J and L shapes and T shapes, and are least soluble in the S and Z fluids. The S, Z, and T shapes are all mutually quite soluble, with S and Z being slightly more soluble in the T fluid than in each other and T being more soluble in the S and Z fluids than in any other. This appears to be due to the strong similarity of these shapes, which share a “stepped” motif. We also see evidence of chiral interactions in the solubilities of J and L in the S and Z fluids and vice versa. The solubility of S in L is the same as that of Z in J, and the J–Z (or L–S) pair is more mutually soluble than the J–S (or L–Z).

In the near-equimolar binary mixtures, the solubility of other shapes is generally intermediate between the solubilities in the corresponding pure fluids. For instance, squares are less soluble in the S/J mixture than in the pure J fluid, but more soluble than in the pure S fluid. This is consistent with the clustering behavior seen earlier, which suggests that, to a solute, the mixture looks like small regions of pure fluids. In a few cases, such as J dissolved in the O/T mixture, shapes are as soluble in the mixture as in one of its components. In this case, the poor structural compatibility of the O and T fluids and their relatively large volume of mixing provide many voids into which the solute may fit. In one particularly interesting case, the L shape is noticeably more soluble in the S/J mixture than in either of the pure S or J fluids. There is a large positive volume of mixing in the S/J system, which is the likely cause.

In the “senary” row of Table 4 are shown the solubilities of each shape in the six-component mixture of the remaining shapes, again all at equal chemical potentials such that $\beta p = 0.5$. For comparison, the averages of the solubilities of each shape in the six other pure solvents are given in the last row. In all cases, the six-component mixture is a better solvent than one might expect from averaging over its components, although the difference is relatively small. Also, the trend established in the pure fluids remains, with squares being the most soluble of the shapes and rods being the least soluble.

Finally, we note that the ratio of the $1/\beta K_i$ values for a species i in two different solvents is a partition coefficient which describes the distribution of a solute between them. At this pressure, the largest partition coefficient is for rods dissolved in square and Z (or S) solvents, with $K_I(O/Z) = 1.49$, a relatively modest preference for the fluid of squares. As the pressure is increased, the total solubilities decrease, but the partition coefficients can be greater; at $\beta p = 1.00$, $K_I(O/Z) = 2.14$, but the solubilities are reduced to 0.015 in the fluid of squares and to 0.007 in the Z fluid.

4. Discussion

The simulations described above provide a detailed picture of the structure and thermodynamics of both the single-component fluids and binary mixtures, as well as some insight into the behavior of many-component mixtures. The tetromino fluids do not display sharp (first-order) phase transitions in the density range studied, although there remains the possibility of continuous phase transitions without divergences in the compressibility or other signatures. However, they do display intriguing local structure, including clustering of like-oriented pieces in the pure fluids and localized strong species segregation in binary and multicomponent mixtures. That is, although only purely entropic forces are present in these systems, pieces appear to preferentially associate with other pieces of the same shape and complementary (although not necessarily identical) orientation.

The qualitative picture of these interactions obtained through inspection of representative configurations is supported by analysis of several quantitative measures, including second virial coefficients, volumes of mixing, cluster size statistics, and solubilities in the form of Henry’s law constants. While related models have been used in a number of other simulation studies, the structure of the fluids and the associated thermodynamics have not been considered in any detail, and multicomponent mixtures have not been treated in any previous study of which we are aware.

Although the structures adopted in the fluids of squares and rods are reasonably intuitive, the behavior of the remaining pieces is rather less so. All of the tetrominoes can be used to completely cover the lattice (100% packing) in a combinatorially large number of ways, including via well-ordered periodic structures. The structures of the J, L, and T fluids, although successfully rationalized in terms of piece–piece interactions, are not easily predicted, and one can easily imagine other structural motifs for packing these shapes at high densities. It thus appears that using shape alone to direct self-assembly is perhaps more difficult than it might appear, because rather surprising behavior is observed even among such simple shapes.

The preference for association of pieces of like shape and complementary orientation, the solubilities of each species in the other fluids, and the volume of mixing data can all be interpreted via the usual chemical rule of thumb that “like dissolves like”, provided that one has an expansive interpretation of “like”. Consider, for instance, that squares and rods are the most and least compact of the shapes studied, yet are quite mutually soluble, while rods and J shapes are much less soluble in each other. Solubility is controlled by the compatibility of the solute with the characteristic structures formed in the solvent, rather than with the solvent pieces themselves. Squares are very soluble in the dense J fluid because the J pieces tend to pair, forming compact 2×4 site structures, and a fluid of such structures is amenable to forming 2×2 site vacancies, which exactly fit a square. Rods are much less soluble in the J fluid than are squares, despite “looking” more like J pieces than squares do, because the 1×4 vacancy required to accommodate a rod requires a larger perturbation of the structure of the J fluid. Another type of compatibility occurs in fluid mixtures, between the characteristic structures formed by both shapes. Squares and rods have only modestly positive volume of mixing even at high densities, because both pieces form structures faceted along the Cartesian lattice vectors. S and Z shapes have nearly zero volume of mixing and display significant microscopic segregation, because they both form structures faceted along the lattice diagonals. Squares and S shapes, however, exhibit the most positive volume of mixing of any two species, due to the extreme incompatibility of their characteristic structures; rods and S shapes are nearly as incompatible.

It remains curious that in all of the mixtures considered each shape prefers to associate with its own type rather than with any combination of others. One possible explanation for this behavior is that the tetrominoes are quite thin (either one or two lattice sites), and so their “face” on one side tends to be the same as that on the other; this is true for all the shapes except the T. This would lead to a natural tendency for shapes to pack efficiently in the same orientation, which is observed for the rods and S and Z shapes. J and L shapes also pack this way, but only at low densities; at high densities they rotate to make contact with the same face on another piece. T shapes form the most complex structures at high density, perhaps because they are unlike the other pieces in not having opposing

faces of similar shape. Self-association is likely not a general feature of polyomino fluids; one can easily imagine larger shapes that exhibit “lock and key” shape complementarity or frustrated structures that cannot pack efficiently with themselves.⁵³

Much of this behavior can be predicted qualitatively by examination of second virial coefficients. The orientationally averaged “thermodynamic” coefficients defined in eq 2 do not provide much insight into the fluid structure, but the orientation-specific coefficients correlate extremely well with behavior observed in the simulations. In nearly all cases, the relative orientations adopted by pieces in the dense fluids are those with the lowest orientation-specific coefficients. This suggests that these quantities may be useful in designing shapes that will exhibit a particular structure or packing motif; this should be equally true in systems that exhibit attractive interactions.

Increasing the number of components in a mixture decreases the tendency of each species to self-associate. This appears to be principally due to dilution, rather than any tendency for shapes to form characteristic multicomponent structures. Analysis of Henry’s law data indicates that some many-component mixtures are generally better solvents (for shapes not present in the mixture) than are pure species or binary mixtures. Much of this behavior can be correlated with the volume of mixing in the solvent; when the solvent components do not mix well, the density of the fluid is lower (at a given pressure) than otherwise, and it becomes a better solvent for other species because it has more empty space available. Such a correlation is likely to be present for other polyominoes, and perhaps real colloidal and nanoparticulate systems, and may suggest routes toward the systematic control of solvation behavior in such systems.

All of the fluids studied are fully miscible; no macroscopic phase separation was ever observed in these simulations. In off-lattice hard models, even in two dimensions, this is not always the case. For instance, demixing can be observed in mixtures of hard rectangles and disks or discorectangles.¹⁷ Again, we expect that such phenomena may be observed in other (on-lattice) multi-component polyomino fluids, especially when components are of substantially different size. Because an isotropic-to-nematic transition has already been identified for on-lattice rods of lengths greater than considered here,⁴⁸ we believe that many single-component and multicomponent fluids of larger polyominoes are likely to exhibit true phase transitions. Extension of the model to three dimensions would increase the number of rotational states available and thus increase the likelihood of observing first-order transitions.

The off-lattice counterparts of some of the shapes considered here have been studied by other groups.^{15–18,48} On- and off-lattice models behave quite differently, but this is not surprising. In the off-lattice model, especially at high densities, the free energy of the fluid is principally determined by free volume considerations, and the structure adopted is one that maximizes the ability of individual objects to move about within the confinement of their neighbors. In the lattice model studied here, there is very little opportunity for such small-amplitude motions at high densities. Most importantly, the orientational degree of freedom in the lattice model is discrete, with very few states available, so that the total entropy is dominated by translational terms; this is not the case in the off-lattice systems.

In conclusion, we have observed a number of interesting and previously unexplored phenomena in simulations of an idealized model with relevance to molecular adsorption and self-assembly in two dimensions. The extreme simplicity of the shapes studied and their interactions belies considerable complexity and

nonideality in the structure of the simulated fluids and mixtures. Quantities such as second virial coefficients, familiar from the analysis of simple liquids, and rigorous solution thermodynamics can nonetheless be used to correlate and understand most of this behavior. Larger polyominoes may exhibit true phase transitions, long-range ordering, and even more complex behavior, and will be a topic of future study. We note in this regard that, even with an inexpensive model such as this and an efficient computer implementation, an exhaustive search of a high-dimensional phase space is likely beyond current computational capabilities. We are therefore investigating statistical approaches for locating phase transitions in such a space using ideas from quantitative stereology.⁵⁴ Tetrominoes confined in small spaces may be induced to exhibit regular structure. If the confinement reinforces the characteristic structure of a fluid it will be enhanced, perhaps leading to pseudocrystallization; on the other hand, an incompatible confinement geometry may be used to enhance fluid mixing. Confinement might also be used to effect a chromatographic separation based on liquid structure, rather than particle size; this will also be considered in future work. Finally, the results obtained to date may have some relevance to successful strategies for playing the Tetris computer game, but this has not been considered in detail.

Acknowledgment. We acknowledge financial support from the National Science Foundation (CHE-0626008 and CHE-0718861), the ARO (W911NF-07-1-0253), and the Washington University Center for Materials Innovation. Some of these calculations were performed on the NSF Teragrid (allocation MCA08X001).

Appendix

Calculation of Pressure. In the athermal thermodynamics appropriate to this model, the Gibbs–Duhem equation is

$$d\beta p = \sum_i \rho_i d\beta \mu_i \quad (4)$$

Integration yields

$$\beta p(\beta \mu) = \beta p(\beta \mu_0) + \sum_i \int_{\beta \mu_0}^{\beta \mu} \rho_i(\beta \mu') d\beta \mu' \quad (5)$$

(For a system with a real temperature, these expressions are still valid at constant β .) In principle, the integration in eq 5 is path independent (one can integrate through any set of $\beta \mu$ state points). For a pure fluid the path selection is trivial, and the quality of the result depends only on the spacing in $\beta \mu$ between simulations. For each binary mixture of species A and B we have chosen to use rectilinear paths to reach each state point:

$$\begin{aligned} p(\beta \mu_A, \beta \mu_B) &= p(\beta \mu_{A,0}, \beta \mu_{B,0}) + \\ &\quad \int_{\beta \mu_{A,0}}^{\beta \mu_A} \rho_A(\beta \mu'_A, \beta \mu_{B,0}) d\beta \mu'_A + \\ &\quad \int_{\beta \mu_{B,0}}^{\beta \mu_B} \rho_B(\beta \mu_A, \beta \mu'_B) d\beta \mu'_B \end{aligned} \quad (6)$$

(53) Many may consider the tetrominoes already sufficiently frustrating in this regard.

(54) Underwood, E. E. *Quantitative Stereology*; Addison-Wesley: Reading, MA, 1970.

$\beta\mu_{A,0}$ and $\beta\mu_{B,0}$ are chosen such that the density is very low, so that $p(\beta\mu_{A,0}, \beta\mu_{B,0})$ can be accurately computed using the virial equation of state truncated at second order, eq 2. The integration is a two-step process: $\beta\mu_{B,0}$ is held fixed during integration up to the desired $\beta\mu_A$, after which $\beta\mu_A$ is held fixed while $\beta\mu_B$ is varied. Integrations were performed using Simpson's 1/3 integration. We examined different integration paths and found that the variation in βp due to choice of integration path was insignificant, confirming that the simulations are spaced closely enough in $\beta\mu$ to provide reliable thermodynamics.

Calculation of Volume of Mixing. The change in volume upon mixing is defined as

$$\Delta V_{\text{mix}}(\mathbf{N}, \beta p) = V(\mathbf{N}, \beta p) - \sum_i \hat{V}_i(\beta p) N_i \quad (7)$$

where $\hat{V}_i(\beta p)$ is the molar volume of pure species i at pressure βp . Our simulations of binary mixtures were performed in the grand ensemble, which necessitates several additional manipulations to obtain ΔV_{mix} as it is conventionally used, as follows:

- 1 Obtain the equation of state, βp as a function of $\beta\mu$ for each single-component (pure) fluid by thermodynamic integration, as described above.
- 2 For each species i , fit $\hat{V}_i(\beta\mu_i)$ versus $\beta p(\beta\mu_i)$ via a cubic-spline function to provide $\hat{V}_i(\beta p)$.
- 3 Compute βp as a function of the chemical potentials $\beta\mu$ for the desired mixture, again by thermodynamic integration. Combine this with the numbers of each shape $\mathbf{N}(\beta\mu)$, obtained in the simulation, to yield $V(\mathbf{N}, \beta p)$.
- 4 For each state point $\beta\mu$, compute ΔV_{mix} via eq 7 .
- 5 Plot ΔV_{mix} (or $\Delta V_{\text{mix}}/V$) as a function of βp and mole fractions \mathbf{x} .

Calculation of Henry's Law Constants. In an athermal system, in the Henry's law regime

$$\beta f_i^\infty(\beta p, x_i) = x_i \beta K_i(\beta p) \quad (8)$$

that is, the fugacity of species i at infinite dilution in a particular solvent is equal to its mole fraction in the solution multiplied by a constant βK_i , which depends on both the solvent and solute and varies with pressure. βK_i is related to the excess chemical potential of the solute i at infinite dilution by^{55,56}

$$\beta K_i(\beta p) = \rho_s \exp[\beta\mu_{i,\text{ex}}^\infty(\beta p)] \quad (9)$$

where ρ_s is the solvent density. We measure $\beta\mu_{i,\text{ex}}^\infty$ via Widom test-particle insertion.⁵⁷ In the grand canonical ensemble

$$\beta\mu_{i,\text{ex}}^\infty = -\ln\langle\exp(-\beta\Delta U_i)\rangle_{\beta\mu, V} \quad (10)$$

where ΔU_i is the energy associated with the insertion of a test particle of species i in the solvent and the ensemble average is taken over both possible insertion positions (and orientations) and the positions and number of particles of other species present. Note that in the grand ensemble this expression applies only to the solute and not to the components of the solvent. In the hard model studied here, the term in brackets reduces to the ensemble average probability of successfully inserting a test particle of species i in the system when there are no other particles of species i present.

(55) Shing, K. S.; Gubbins, K. E.; Lucas, K. *Mol. Phys.* **1988**, *65*, 1235–1252.

(56) Tester, J. W.; Modell, M. *Thermodynamics and Its Applications*, 3rd ed.; Prentice Hall: Upper Saddle River, NJ, 1996.

(57) Widom, B. *J. Chem. Phys.* **1963**, *39*, 2802–2812.